

Directly Revealing Entanglement Dynamics through Quantum Correlation Transfer Functions with Resultant Demonstration of the Mechanism of Many-Body Localization

Peyman Azodi* and Herschel A. Rabitz

Department of Chemistry, Princeton University, Princeton, New Jersey 08544, USA

(Dated: January 28, 2022)

The fundamental link between entanglement dynamics and non-equilibrium statistics in isolated quantum systems has been established in theory and confirmed via experiment. However, the understanding of several consequential phenomena, such as the Many-Body Localization (MBL), has been obstructed by the lack of a systematic approach to obtain many-body entanglement dynamics. This paper introduces the Quantum Correlation Transfer Function (QCTF) approach to entanglement dynamics in many-body quantum systems and employs this new framework to demonstrate the mechanism of MBL in disordered spin chains. We show that in the QCTF framework, the entanglement dynamics of two-level constituent particles of a many-body quantum system can be fully characterized directly from the system's Hamiltonian, which circumvents the bottleneck of calculating the many-body system's time-evolution. By employing the QCTF-based approach to entanglement dynamics, we demonstrate MBL dynamics in disordered Heisenberg spin chains through the suppressed quasi-periodic spin's entanglement evolution after a quench from an anti-ferromagnetic state. Furthermore, we prove the validity of a previous fundamental conjecture regarding the MBL phase by showing that in strongly-disordered spin chains with short-range interactions, the quantum correlation between particles is exponentially attenuated with respect to the site-to-site distance. Moreover, we obtain the lowest possible amplitude of the quasi-periodic spin's entanglement as a function of disorder in the chain. The QCTF analysis of MBL dynamics is verified by exact numerical simulation of the system's evolution. We also show that QCTF provides a new foundation to study the Eigenstate Thermalization Hypothesis (ETH). The QCTF methodology can be extended in various ways to address general issues regarding non-equilibrium quantum thermodynamics in spin lattices with different geometries.

I. INTRODUCTION

Entanglement is a fundamental property of quantum physics. Despite the long-standing controversy around this phenomenon in the early period of developing quantum mechanics, recent experiments have confirmed the special role of entanglement in quantum statistics by demonstrating thermalization in closed quantum systems [1–3]. These observations support former theoretical speculations on the link between entanglement and statistics in closed quantum systems [4–6], notably the Eigenstate Thermalization Hypothesis (ETH), in which the thermal behavior in an interacting many-body quantum system is attributed to its individual eigenstates [7, 8]. Moreover, this novel viewpoint to quantum statistics allows for explaining certain phenomena, impossible to treat in semi-classical theories in which the pivotal role of entanglement is not taken into consideration [9–11]. As a remarkable example, we highlight the absence of thermalization in disordered chains of quantum particles, known as the Many-Body Localization (MBL) phenomenon [12, 13]. In spite of the established fundamental link between entanglement and statistics in many-body quantum systems, characterizing the dynamics of entanglement has been obstructed by its inherent complexity due to the exponentially large Hilbert space that often

underlie many-body quantum systems. This article targets two important gaps in the literature. First, by introducing a new theoretical framework to characterize entanglement dynamics in many-body quantum systems, and second by employing this new approach to demonstrate the mechanism of MBL. These two objectives will be explained further in this section as background to the paper.

A systematic approach to characterize many-body entanglement dynamics has been built on the work of Holzhey, Larsen, and Wilczek in 1994 [14], and Calabrese and Cardy in 2004 [15], which employs the so-called *replica trick* on a quantum field with conformal symmetry to obtain the entanglement entropy. This approach is analytically solvable for the continuum limit of 1D spin lattices, corresponding to a 1+1d conformal field theory [16, 17], which has led to proving variants of ETH for this class of systems [18, 19]. Nevertheless, systems wherein the conformal symmetry is absent are predominant and of high interest. In the context of conformal field theory several crucial features such as parametric disorder, few-body and edge effects are not possible to treat. These features have been shown to give rise to novel phenomena such as eigenstate phase transitions [20–22], as discussed in the next paragraph. Several aspects of the entanglement behavior in many-body quantum systems have remained unexplored, especially when disorder is present, which is fundamentally important and “notoriously difficult”, as referred to by Ed-

* pazodi@princeton.edu

uardo Fradkin [23]. Thus, given the well-established and unique role of entanglement in the statistics of many-body quantum systems, the first objective of this paper will be to present a new methodology, referred to as the Quantum Correlation Transfer Function (QCTF), to obtain the correlation dynamics directly from the system’s characteristics. Here, the words “directly” refers to bypassing the evaluation of the many-body quantum system’s evolution, which is rarely feasible. Additional comments on this key feature of the QCTF method will be discussed later in this section.

Disorder, or randomness, in the structure of a quantum system can inhibit thermalization. This feature is the essence of Many-Body Localization (MBL), which generalizes the Anderson localization phenomenon [24, 25] to strongly-interacting many-body quantum systems [12, 26]. Extensive numerical studies have confirmed that disordered chains of interacting spins undergo a phase transition at a critical disorder strength from the thermal phase (at the low-disorder limit) to the MBL phase [27–32]. Recently, MBL has also been numerically observed in two [33] and three dimensional disordered lattices [34, 35]. This (eigenstate) phase transition is fundamentally different from conventional thermodynamic phase transitions; the high-disorder side is not a thermodynamic (ergodic) phase, but corresponds to the absence of thermalization [36, 37]. Despite this distinction, the MBL phase transition has been associated with different spectral order parameters across a critical point for particular disordered spin chains [38, 39]. This phenomenon is evident in quench experiments where a quantum system’s behavior, commonly initialized at a non-entangled state, is studied after a sudden change in its Hamiltonian. In this scenario, strongly-interacting spins in a sufficiently disordered chain (in the MBL phase) cease to entangle, when initially uncorrelated [40]. This phenomenon is in contrast to quantum thermal behavior, wherein entanglement develops and saturates between the interacting particles after a quench [1]. Despite several numerical demonstrations of MBL dynamics, the underlying mechanism of MBL has not been theoretically demonstrated. A proposal to explain the MBL in 1D lattices is the quasi-Local Integrals Of Motion (LIOMs) approach, that is contingent on a fundamental conjecture (which we prove correct in this paper). In particular, in the MBL phase, quantum correlations between spins attenuate exponentially with respect to the particle’s site-to-site distance [41–43]. The MBL phenomenon is of exceptional interest due to the absence of such behavior in the classical analogue where non-ergodic trajectories are highly unstable for an interacting classical system [44, 45]. Accordingly, the second objective of this paper is to employ the QCTF approach to demonstrate the mechanism of MBL.

This paper presents a new approach to obtain the correlation dynamics in many-body quantum systems by transforming the unitary time-evolution of the system into a complex-valued function, the QCTF. To this end, a

transformation is defined to encode the system’s dynamics into the analytic properties (i.e., poles and zeros) of the QCTF. By virtue of this transformation, the dynamics of correlations in the many-body quantum system, inherently obscured in the system’s state, can be explicitly revealed through closed-contour integrations in the complex space where the QCTF is defined. We show that this technique provides a foundation to study the ETH by quantifying the entanglement of strongly-interacting many-body eigenstates. Although the QCTF formulation is valid for arbitrary quantum states, the subsequent QCTF-based entanglement analysis in this paper will focus on the class of many-body quantum systems consisting of constituent particles each having two energy levels, i.e., spin- $\frac{1}{2}$ lattices, which are of prime current interest. Therefore, following the first objective of the paper, the formulation of QCTF is introduced and then employed to obtain the entanglement dynamics of spin- $\frac{1}{2}$ particles of generic many-body quantum systems. This *frequency-based* analysis allows for inferring crucial properties of the system’s correlation *dynamics*. Importantly, within the QCTF framework, correlation dynamics is obtained directly from the quantum system’s characteristics, which would otherwise require extensive computational effort using time-domain analysis methods, such as numerical iteration based on exact-diagonalization or the Matrix Product State (MPS) formulations. More precisely, in the QCTF framework we exploit the fact that correlations between the particles of a quantum system emerge as a result of the *relative* evolution of orthogonal amplitudes in the system’s wave function. Therefore, by focusing on, and analyzing these relative evolutions, we circumvent the need to calculate the full time-dependence of the many-body quantum system’s state. The novel QCTF approach is further used to demonstrate the mechanism of MBL in the widely used model of disordered Heisenberg spin chains of arbitrarily length. Employing the QCTF leads to the frequency spectrum of the dynamical entanglement measure in the many-body quantum system. Utilizing this feature, we show that at the high-disorder strength limit (i.e., MBL phase), the frequency spectrum of the quenched entanglement measure is composed of a few dominant components which correspond to the interaction between neighboring sites. Additionally, we employ the Mellin transformation to prove that the residual amplitudes corresponding to interaction with further sites are *exponentially* attenuated in the site distance. This analysis proves the latter pivotal conjecture regarding the MBL phenomenon [41–43]. Furthermore, the QCTF-based approach confirms that in the MBL phase the quenched subsystem’s entanglement is *quasi-periodic* and its amplitude is *lower bounded* as a function of the disorder strength. We verify the validity of the QCTF formulation with numerical simulation of the MBL dynamics in disordered Heisenberg chains of computationally feasible length.

The remainder of this paper is organized as follows. In Section II, the general principles of the QCTF framework

are presented and the basic form of the QCTF is introduced. Section III utilizes a QCTF-based analysis to reveal the entanglement dynamics of interacting two-level particles of a many-body quantum system. In this section, the particle's entanglement of the system's generic many-body eigenstates is characterized in terms of the properties of the corresponding quantum system. Section IV presents a detailed analysis of the MBL phase in disordered spin chains. In Subsection IV A time-independent perturbation theory is employed to obtain the QCTF formulation of strongly-disordered Heisenberg spin chains. Accordingly, the entanglement evolution of spins is derived and the MBL dynamics is demonstrated. In Subsection IV B, the Mellin transformation is employed to prove the aforementioned conjecture on exponential decay of correlations in the MBL phase with respect to inter-particle distances. Subsection IV C includes numerical verification of the theoretical QCTF analysis of the MBL dynamics. Concluding remarks are given in section V, where we also suggest a path for further development and applications of the QCTF. Note that each figure's caption contains extensive explanatory material complementary to the main text. Finally, mathematical derivations and proofs of key results in the main text are given in the Appendix.

II. BASIC FORMULATION OF THE QCTF

The evolution of a quantum system in this formulation is described via a complex function, i.e. the QCTF, through what we refer to as chronological and structural frequency components. The chronological frequency component describes the system's time dependence, while the structural frequencies encode the variation of the system's state, in an arbitrary basis for the underlying Hilbert space. In this formulation, evolution of correlations between the constituent particles of the many-body quantum system can be obtained by integrating the QCTF along certain closed contours in the structural frequency space. We specify the basic QCTF transformation of the system's density matrix in Subsec-

tion II A, with special focus on the important case of pure quantum states in Subsection II B.

A. QCTF transformation of the system's density matrix

For a generic quantum system with discrete energy levels, the basic QCTF is defined via the following 2-variable transformation of the element-wise Laplace-transform of the density matrix, $\tilde{\rho}(s) = \mathcal{L}\{\rho(t)\}$, as

$$\mathcal{K}(z_d, z_a, s) = \sum_{l,k=0}^{d-1} \langle l|\tilde{\rho}(s)|k\rangle z_d^{l-k} z_a^{l+k}, \quad (1)$$

where d is the quantum system's Hilbert space dimension and $\{|l\rangle | l = 0, \dots, d-1\}$ is an arbitrary basis for this space. Here the complex variables z_d and z_a are structural frequencies, which are conjugate to the diagonal ($l-k = \text{const.}$) and anti-diagonal ($l+k = \text{const.}$) arrays of elements in the corresponding density matrix, as illustrated and discussed further in Figure 1. The Hermiticity of the density matrix leads to the following symmetry of the QCTF

$$\mathcal{K}(z_d, z_a, s) = \mathcal{K}^*(1/z_d^*, z_a^*, s^*). \quad (2)$$

Equation (1) is the dual Laurent series expansions of \mathcal{K} , in both z_d and z_a variables, centered at the origins of the spaces. Based on the labeling $l = 0, \dots, d-1$ for the Hilbert space basis, the origin $z_d = 0$ is a pole of order (at most) $d-1$, while the origin $z_a = 0$ is a removable singularity in the z_a space. Also, for finite d , the function \mathcal{K} is holomorphic in any punctured neighbourhood of the origin, in both structural spaces.

The QCTF (1) provides an equivalent description for the evolution of a quantum system as its density matrix, $\rho(t)$. To confirm this statement, given any arbitrary basis set $\{|l'\rangle\}$ and arbitrary time $t' > 0$, the transition amplitude $\langle l'|\rho(t')|k'\rangle$ can be obtained from the QCTF (1) through the following inverse transformation via close-contour integrations in \mathbb{C}^3 (refer to Appendix A for the proof)

$$\langle l'|\rho(t')|k'\rangle = \frac{1}{(2\pi i)^3} \oint_{\partial C_s} ds \oint_{\partial C_d} dz_d \oint_{\partial C_a} dz_a e^{st'} \sum_{l,k} \langle k|k'\rangle \langle l'|l\rangle z_d^{-(l-k)-1} z_a^{-(l+k)-1} \mathcal{K}(z_d, z_a, s), \quad (3)$$

where $\partial C_{a(d)}$ is any counter-clock-wise (CCW) closed curve in the $z_{a(d)}$ planes enclosing the origin, wherein \mathcal{K} is holomorphic except at $z_{a(d)} = 0$, and ∂C_s is any CCW closed curve enclosing all of the poles of \mathcal{K} on the imaginary axis of the s domain. In principle, any generic density matrix can be transformed into its QCTF representation. This property allows for describing the evolu-

tion of quantum systems with time-dependent Hamiltonian via the QCTF formulation. The remainder of this paper will consider time-independent Hamiltonians, particularly due to their high importance in various current scenarios of many-body quantum statistical mechanics. In summary, the QCTF fully represents an arbitrary density matrix and in the next sections of this paper we will

exploit this equivalence to reveal quantum statistical features of many-body systems in the QCTF framework.

B. QCTF for pure quantum systems

In this subsection, we will focus on the important case of pure state quantum systems ($\rho = |\psi\rangle\langle\psi|$). For this purpose, consider the unitary evolution of the initial state $|\psi_0\rangle$ under Hamiltonian \mathbf{H} . Accordingly, we can define the following 1-parameter QCTF transformation, denoted by $\bar{\mathcal{K}}$, of the system's wave-function in the Laplace domain ($|\tilde{\psi}(s)\rangle = \mathcal{L}\{|\psi(t)\rangle\}$) as follows:

$$\begin{aligned}\bar{\mathcal{K}}(z, s) &= \sum_{l=0}^{d-1} z^l \langle l | \tilde{\psi}(s) \rangle \\ &= \sum_{l=0}^{d-1} z^l \langle l | \mathbf{G}(s) | \psi_0 \rangle,\end{aligned}\quad (4)$$

where $\mathbf{G}(s) = (s + \frac{i}{\hbar}\mathbf{H})^{-1}$ is the resolvent of the system. In this case, the basic QCTF (1) can be directly obtained (refer to Appendix B for details) as

$$\mathcal{K}(z_d, z_a, s) \doteq \bar{\mathcal{K}}(z_d z_a, s) \star \bar{\mathcal{K}}^*((z_a/z_d)^*, s^*), \quad (5)$$

where operation \star is defined by the ordinary product operation in the z_d and z_a domains and the following convolution operation in the s domain. If $\mathbf{F}_1(s)$ and $\mathbf{F}_2(s)$ are functions in the Laplace domain, then:

$$\mathbf{F}_1(s) \star \mathbf{F}_2(s) \doteq \frac{1}{2\pi i} \int_{-\infty}^{\infty} \mathbf{F}_1(\sigma + i\omega) \mathbf{F}_2(s - \sigma - i\omega) d\omega, \quad (6)$$

for some real σ in the region of convergence (ROC) of $\mathbf{F}_1(s)$. As an important special case of equation (6), we have $(s + i\omega_1)^{-1} \star (s + i\omega_2)^{-1} = (s + i(\omega_1 + \omega_2))^{-1}$.

More generally, the dynamics of a pure quantum system evolving under the Hamiltonian \mathbf{H} can be represented by an operator function $\mathcal{H}(\mathbf{H}, z_d, z_a, s)$, which includes its dynamical correlation properties, independent of its initial state. To see this, using definition (5), the QCTF transformation can be rewritten as the expectation value of \mathcal{H} with respect to the arbitrary initial state ($|\psi_0\rangle$),

$$\mathcal{K}(z_d, z_a, s) = \langle \psi_0 | \mathcal{H}(\mathbf{H}, z_d, z_a, s) | \psi_0 \rangle, \quad (7a)$$

$$\mathcal{H} = \mathbf{G}^\dagger(s^*) \left(\sum_{l,k} z_a^{l+k} z_d^{l-k} |k\rangle \langle l| \right) \star \mathbf{G}(s). \quad (7b)$$

The operator \mathcal{H} includes the dynamical properties of the quantum system, including the evolution of correlation between its constituent particles. This property, which will be discussed in detail in the next section, can be employed to understand how the correlation behavior varies for different initial states of the quantum system.

In the QCTF formulation, the general approach to obtain the many-body quantum system's properties (e.g., the correlation dynamics between the particles) is to integrate a function of the QCTF (4) around appropriate closed contours in the structural frequency spaces. Equation (3) is an example of this procedure to obtain the system's density matrix elements. Given the fact that QCTF is an equivalent representation of the system's density matrix, in principle it is possible to obtain the dynamics of various forms of correlation, such as two-particle correlations, higher-order (multi-particle) correlations and particle's entanglement (the subject of the next section), by integrating a suitable function of the QCTF.

III. ENTANGLEMENT DYNAMICS IN THE QCTF FORMULATION

In this section, the QCTF approach is employed to characterize the entanglement evolution of two-level particles of a generic (many-body) quantum system which is initialized at a pure state and evolves unitarily. First, we introduce the entanglement measure used in the analysis and then we obtain the time evolution (dynamics) of the measure from the quantum system's QCTF.

Consider a closed quantum system with discrete energy levels, consisting of a two-level particle (referred to as subsystem \mathcal{M}) that interacts with an accompanying d -dimensional quantum subsystem \mathcal{R} . The bipartite quantum system evolves according to the Hamiltonian \mathbf{H} from the initial state $|\psi_0\rangle = |\psi(t=0)\rangle$. If we denote the reduced density matrix of the subsystem \mathcal{M} by $\rho_{\mathcal{M}}(t) = \text{Tr}_{\mathcal{R}}\{|\psi(t)\rangle\langle\psi(t)|\}$, then $\mathcal{Q}_{\mathcal{M}}(t) = \det(\rho_{\mathcal{M}}(t))$ is a time-dependent entanglement measure of subsystem \mathcal{M} , which is also monotonically related to the second-order Rényi entanglement entropy through $\mathcal{S}_2(\mathcal{M}) = -\ln(1 - 2\mathcal{Q}_{\mathcal{M}})$. Equivalently, we will use its Laplace transformation $\tilde{\mathcal{Q}}_{\mathcal{M}}(s) = \mathcal{L}\{\mathcal{Q}_{\mathcal{M}}(t)\}$ as the *dynamical entanglement measure* in the analysis.

The entanglement measure $\tilde{\mathcal{Q}}_{\mathcal{M}}(s)$ can be obtained from the QCTF, which is now defined on an off-diagonal block of the system's density matrix, $\tilde{\rho}(s)$. Given any basis for the quantum system which is constructed from the *arbitrary* basis vectors $\{|+\rangle, |-\rangle\}$ for \mathcal{M} and $\{|l\rangle, l = 0, \dots, d-1\}$ (d can be countably infinite) for \mathcal{R} , we define the QCTF on the off-diagonal block $\langle + | \tilde{\rho}(s) | - \rangle$, as follows,

$$\mathcal{H} = \mathbf{G}^\dagger(s^*) \left(\sum_{l,k} z_a^{l+k} z_d^{l-k} |-\otimes k\rangle \langle +\otimes l| \right) \star \mathbf{G}(s), \quad (8a)$$

$$\mathcal{K}(z_d, z_a, s) = \langle \psi_0 | \mathcal{H} | \psi_0 \rangle. \quad (8b)$$

Having introduced the suitable form of QCTF for the purpose of this section, in Appendix C we prove that

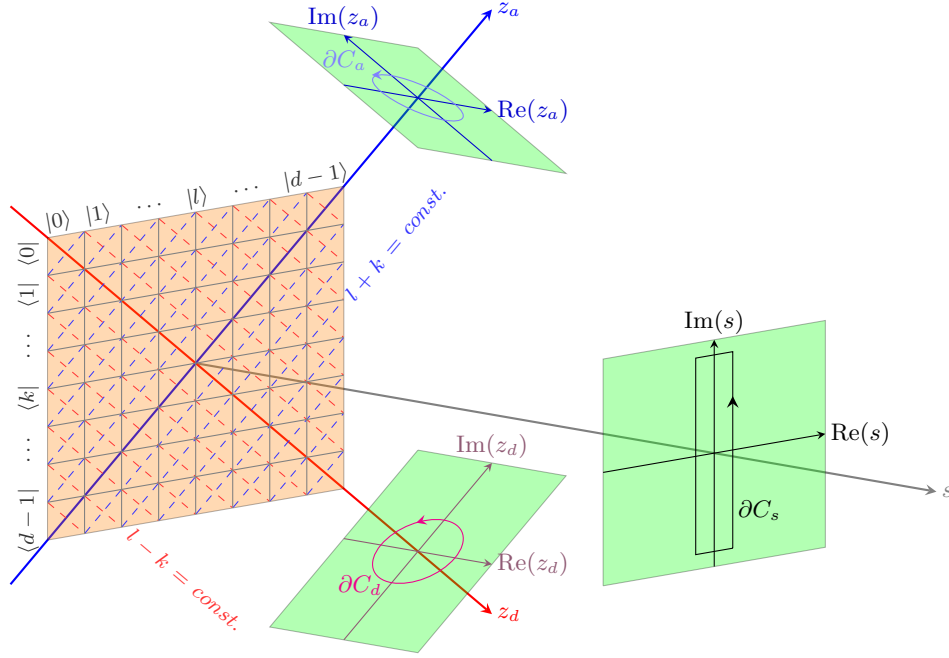


FIG. 1. Schematic illustration of the QCTF transformation in (1). This illustration shows how the QCTF transformation (1) relates different frequency spaces, z_d , z_a and s (each depicted in green) to the time-dependent density matrix (depicted in orange and labeled by quantum indices). For the case of pure states, column l (row k) of the density matrix ρ , corresponds to the (conjugated) time-dependent system's wave-function, projected on the basis vector $|l\rangle$ ($|k\rangle$). The QCTF transformation is achieved by mapping the density matrix into the structural (z_d , z_a) and chronological (s) spaces so that a pole in the s space is defined along with its structural dependence. Typically, the QCTF is a non-separable function of its argument frequencies. The dependence of elements in the density matrix which are parallel to the diagonal is encoded into the complex z_d space. This structural part of the transformation maps all of the described elements (constant $l-k$) with a same exponent z_d^{l-k} . The other structural frequency of the QCTF transformation, z_a , is analogously depicted in blue color, which maps the elements on anti-diagonal rays (constant $l+k$) with the same corresponding exponent z_a^{l+k} . The counterclockwise closed contour ∂C_d (depicted in magenta), over which the QCTF is integrated, encloses the origin of this space. A similar remark applies to the closed contour ∂C_a (depicted in light blue). The s axis (depicted in gray) corresponds to the element-wise Laplace transformation of the density matrix into the s space. The poles in this space are located on the imaginary axis, due to the unitarity of the time evolution. The counterclockwise closed contour ∂C_s is depicted in black and encloses all of the chronological poles of the QCTF.

the dynamical entanglement measure ($\tilde{Q}_{\mathcal{M}}(s)$) can be obtained from the QCTF (8b) as follows,

$$\tilde{Q}_{\mathcal{M}}(s) = (2\pi i)^{-2} \oint_{\partial C_d} \mathbf{d}z_d \oint_{\partial C_a} \mathbf{d}z_a \left[(z_d z_a)^{-1} \mathcal{K}(z_d, z_a, s) \star \mathcal{K}^*(1/z_d^*, 1/z_a^*, s^*) \right] - \mathcal{K}_d(z_a, s) \star \mathcal{K}_d^*(1/z_a^*, s^*) \Big|_{z_a=1}, \quad (9)$$

with $\mathcal{K}_d(z_a, s) \doteq (2\pi i)^{-1} \oint_{\partial C_d} \mathbf{d}z_d [z_d^{-1} \mathcal{K}(z_d, z_a, s)]$.

Here $\partial C_{d(a)}$ are closed CCW contours where the integrands are holomorphic except at the origin of the $z_{d(a)}$ planes. The first term in (9) corresponds to the Frobenius norm of the off-diagonal sub-matrix $\langle +|\tilde{\rho}(s)|-\rangle$, while the second term corresponds to the summation of the cross-correlation of its diagonal. These two quantities are identical when the subsystems \mathcal{M} and \mathcal{R} are not entangled.

To demonstrate this result, we characterize the static

entanglement measure, $\tilde{Q}_{\mathcal{M}}$, for the particular case when the many-body quantum system is initialized at one of its eigenstates ($|A\rangle$), with energy E_A (therefore we have $\mathbf{G}(s)|A\rangle = (s + \frac{iE_A}{\hbar})^{-1}|A\rangle$). To this end, using the arbitrary product basis $|\pm l\rangle$ for the system, introduced previously in this section, $|A\rangle$ is expanded as (note that $|\pm l\rangle$

and $|\pm\rangle \otimes |l\rangle$ are used interchangeably),

$$\begin{aligned}
|A\rangle &= \sum_{l=0}^{d-1} \underbrace{\langle +l|A\rangle}_{c_l^+} |l\rangle + \sum_{l=0}^{d-1} \underbrace{\langle -l|A\rangle}_{c_l^-} |l\rangle \\
&= |+\rangle \otimes \underbrace{\sum_{l=0}^{d-1} c_l^+ |l\rangle}_{\alpha^+ |A^+} + |-\rangle \otimes \underbrace{\sum_{l=0}^{d-1} c_l^- |l\rangle}_{\alpha^- |A^-} \\
&= \alpha^+ |+\rangle \otimes |A^+ \rangle + \alpha^- |-\rangle \otimes |A^- \rangle,
\end{aligned} \tag{10}$$

where $\alpha^\pm = \sqrt{\sum |c_l^\pm|^2}$ and $|\alpha^+|^2 + |\alpha^-|^2 = 1$. It is convenient to construct a new basis set, $\{|\tilde{l}\rangle\}$, for the subsystem \mathcal{R} such that $|A^+\rangle$ is one of the basis kets; more precisely, we assign $|\tilde{0}\rangle = |A^+\rangle$ (this procedure is always possible, for instance by using the Gram-Schmidt algorithm, starting from $|A^+\rangle$). Note that without loss of generality, it is assumed that $\alpha^+ \neq 0$.

Due to orthogonality of the new basis set, we have $\langle +\tilde{l}|A\rangle = \alpha^+ \delta_{\tilde{l}0}$. The QCTF can be obtained from (8a-8b) as follows,

$$\mathcal{K}(z_d, z_a, s) = s^{-1} \alpha^+ \alpha^{-*} \sum_{\tilde{k}} (z_a/z_d)^{\tilde{k}} \langle A^- | \tilde{k} \rangle. \tag{11}$$

Consequently, based on equation (9), the entanglement measure $\tilde{Q}_{\mathcal{M}}(s)$ is

$$\begin{aligned}
\tilde{Q}_{\mathcal{M}}(s) &= s^{-1} |\alpha^+ \alpha^-|^2 \sum_{\tilde{k}} |\langle A^- | \tilde{k} \rangle|^2 \\
&\quad - s^{-1} |\alpha^+ \alpha^-|^2 |\langle A^- | A^+ \rangle|^2 \\
&= s^{-1} |\alpha^+ \alpha^-|^2 (1 - |\langle A^- | A^+ \rangle|^2),
\end{aligned} \tag{12}$$

where the completeness relation is used in the last step. The chronological frequency dependence s^{-1} corresponds to the unit step function at $t = 0$ in the time domain, which emphasizes the absence of any time-dependence in the entanglement measure. Based on $\tilde{Q}_{\mathcal{M}}(s)$, the subsystem's entanglement is characterized by the parameters $|\langle A^- | A^+ \rangle|$ and α^+, α^- . Note that no assumption is made about the nature of the quantum system or the eigenstate $|A\rangle$, and this equation holds in general.

To demonstrate how this formulation can be employed to study the ETH, now consider a general many-body quantum system consisting of strongly-interacting particles. The term $|\langle A^- | A^+ \rangle|$ in (12) measures the non-locality of $|A\rangle$ at \mathcal{M} (refer to Appendix D for details). Therefore in a strongly-interacting quantum system with non-local eigenstates (e.g. eigenstates of translationally-invariant lattices) we expect that $|\langle A^- | A^+ \rangle| \ll 1$. Additionally, since the basis $\{|+\rangle, |-\rangle\}$ is chosen arbitrarily, for the systems with spin symmetry, e.g., $\mathfrak{su}(2)$, variables $|\alpha^+|$ and $|\alpha^-|$ must be non-zero (with a significant concentration around $|\alpha^+| \approx |\alpha^-| \approx 1/\sqrt{2}$, that corresponds to the maximal entanglement, $\tilde{Q}_{\mathcal{M}}(s) \approx \frac{s^{-1}}{4}$) for

almost all of the many-body eigenstates. This property is a general manifestation of the ETH. As a result, by relating the statistics of $|\langle A^- | A^+ \rangle|$ and α^\pm to symmetries, the real-space (lattice) dimensionality as well as the range of interactions in the system, a detailed characterization of the entanglement of many-body eigenstates can be achieved.

In summary, this section developed a QCTF-based approach to characterize the entanglement dynamics of the two-level particles in a many-body quantum system. As demonstrated, one form of utilizing this tool is through obtaining the exact QCTF. In the next section, the QCTF is used in a perturbative framework to demonstrate MBL dynamics in a disordered spin chain.

IV. MANY-BODY LOCALIZATION IN DISORDERED HEISENBERG SPIN CHAINS

In this section, the QCTF approach is employed to study MBL dynamics in a disordered chain of strongly-interacting spins. Here we consider the Heisenberg spin chain with nearest-neighbor interactions, initialized at one of the anti-ferromagnetic states, which is the model primarily used in MBL studies [36].

Consider N spin- $\frac{1}{2}$ particles in a one-dimensional lattice with nearest-neighbor spin-spin (exchange) interactions. Additionally, random magnetic fields are introduced at the position of each site, which initiate disorder in the lattice. The Hamiltonian of the closed quantum system is

$$\mathbf{H} = \underbrace{J \sum_{k=1}^{N-1} \mathbf{S}_k \mathbf{S}_{k+1}}_{\text{Interaction (perturbation)}} + \underbrace{\sum_{k=1}^N h_k S_k^z}_{\text{Disorder}}, \tag{13}$$

where $\mathbf{S}_k = \{S_k^z, S_k^x, S_k^y\}$ is the spin operator of the k th particle, J is the nearest neighbor coupling strength and the h_k 's are random and independent fields drawn from the probability density $P_h(x)$. Based upon prior numerical exploration, it has been conjectured in the limit $N \rightarrow \infty$, when $P_h(x)$ is the uniform distribution on the interval $[-W, W]$ then the disordered chain undergoes a MBL transition at a critical disorder strength W_c , which separates the thermal and MBL phases [46]. The dynamics of the spin's entanglement is the feature that distinguishes these two phases when the system is initialized at certain product states. In the thermal phase, each spin's entanglement converges to a saturation value, while the MBL phase is characterized by suppressed [28], and quasi-periodic (as will be demonstrated in this section) dynamics of the spin's entanglement.

Numerical studies have located the critical disorder strength of this system to be in interval $3.5 \leq W_c < 4$ [47, 48]. In what follows, the large disorder (MBL) limit is analyzed via the QCTF approach.

Subsection IV A begins the analysis of the MBL phase of (13) by obtaining its perturbative QCTF representa-

tion. We consider the interaction Hamiltonian as the perturbation to the disorder Hamiltonian in (13). Accordingly, using equation (9), we characterize the entanglement dynamics of spins in terms of Probability Density Functions (PDF) for their frequencies and corresponding amplitudes. In Subsection IV B, we prove that the frequency components corresponding to higher order perturbations are exponentially small in amplitude, which indicates the strong convergence of the perturbation series. Lastly, we test our results in Subsection IV C in two ways. First, we compare the numerically obtained entanglement evolution in a chain of fifteen spins with the predictions from the QCTF formulation. Second, we reconstruct the theoretically derived PDFs from one million simulation samples of spin chains of length six.

A. Perturbative derivation of the entanglement measure

Here we employ time-independent perturbation theory along with the QCTF formulation to analyze the entanglement dynamics of spins in bulk (i.e., far from the edges) of the chain (13). In the MBL phase, the eigenstates of the Hamiltonian (13) are dressed product states from the local eigenstates $|\uparrow\rangle, |\downarrow\rangle$ of σ_z . These product states, which are also the eigenstates of the unperturbed (disordered) Hamiltonian, are used as the basis set $\{|l\rangle\}$ of the QCTF transformation. Therefore, the set of direct product states $\{|\uparrow\rangle, |\downarrow\rangle\}_{\mathcal{M}} \otimes \{|l\rangle\}$ spans the system's Hilbert space. The quantum system is initially in the anti-ferromagnetic state $|\uparrow\downarrow\uparrow\downarrow\cdots\rangle$. Without loss of generality, we assume that the chosen spin (subsystem \mathcal{M}) is initially in state $|\uparrow\rangle$; Let us denote the anti-ferromagnetic state by $|\uparrow 0\rangle$. Similarly, we label some of the product states as shown in Figure 2. For simplicity, we use the notations $\mathbf{J}_k = \mathbf{J}\mathbf{S}_k\mathbf{S}_{k+1}$ and $\mathbf{J} = \sum \mathbf{J}_k$.

The unperturbed resolvent can now be written as

$$\begin{aligned} \mathbf{G}^0 &= (s + \frac{i}{\hbar}E_{\uparrow 0})^{-1} |\uparrow 0\rangle\langle\uparrow 0| \\ &+ (s + \frac{i}{\hbar}E_{\downarrow 1})^{-1} |\downarrow 1\rangle\langle\downarrow 1| \\ &+ (s + \frac{i}{\hbar}E_{\downarrow -1})^{-1} |\downarrow -1\rangle\langle\downarrow -1| + \cdots, \end{aligned} \quad (14)$$

where E_{al} are unperturbed energies, which are simply obtained from the h_k 's. This unperturbed resolvent has

$$\tilde{\mathcal{Q}}_{\mathcal{M}}(s) = \sum_{l,k}' \sum_{i,j,i',j'} c_{i0}^* c_{il} c_{j0} c_{jk}^* c_{i'0} c_{i'l}^* c_{j'0}^* c_{j'k} (s + \frac{i}{\hbar}(E_i^{(1)} - E_j^{(1)} - E_{i'}^{(1)} + E_{j'}^{(1)}))^{-1}. \quad (17)$$

Utilizing this equation, the minimum order of perturbation in $\tilde{\mathcal{Q}}$ for a particular set of l and k is equal to $2(|l| + |k|)$, which is always an even number (refer to

2^N terms corresponding to each of its poles; here we explicitly show three of them. This resolvent does not entangle \mathcal{M} to \mathcal{R} , when the system is initially at the anti-ferromagnetic state. In the remainder of this section, we analyze the effect of perturbations to this resolvent on the entanglement dynamics of \mathcal{M} . For this purpose, we study the interference of product states due to the perturbation (interaction) Hamiltonian \mathbf{J} . To this end, we inspect the transition amplitudes between the product states, caused by individual interaction Hamiltonians \mathbf{J}_k , as shown in Figure 2. We denote the state $|al\rangle$, by $|l\rangle$ in the rest of this section (This is possible because the structure of the interactions prohibits the interference of both $|\uparrow l\rangle$ and $|\downarrow l\rangle$, with the anti-ferromagnetic state ($|\uparrow 0\rangle$) during the perturbation process, which is achieved by applying a set of ordered perturbation Hamiltonians $\{\mathbf{J}_k\}$ consecutively. Importantly, this property implies that the diagonal part of the QCTF, \mathcal{K}_d in (9), vanishes). The interference amplitude between the eigenstates j and i during the perturbation process is denoted by c_{ij} . To obtain these amplitudes, the shortest path between these states (in terms of the number of perturbation steps) is considered. Therefore, for the states shown in Figure 2 we can write $c_{ji} = \frac{\langle i|\mathbf{J}|i+1\rangle\cdots\langle j-1|\mathbf{J}|j\rangle}{(E_i - E_{i+1})\cdots(E_j - E_{j-1})} = c_{jj-1}\cdots c_{i+1i}$ for $i < j$, $c_{ji} = c_{ij}^*$ for $j < i$ and we set $c_{jj} = 1$. As a result, the o^{th} -order perturbed eigenstate $|j\rangle^o$, $j = -3, \dots, 3$ has the following expansion,

$$|j\rangle^{(o)} = \sum_{|i-j|\leq o, i=-3, \dots, 3} c_{ji} |i\rangle. \quad (15)$$

Using (15), the perturbed resolvent can be obtained from (14). Accordingly, using equations (8a-8b), the QCTF is obtained as:

$$\begin{aligned} \mathcal{K}(z_d, z_a, s) &= \sum_{l,k}' z_a^{l+k} z_d^{l-k} \sum_{i,j} c_{i0}^* c_{il} c_{j0} c_{jk}^* (s + \frac{i}{\hbar}(E_i^{(1)} - E_j^{(1)}))^{-1}, \end{aligned} \quad (16)$$

where \sum' denotes the summation over l 's and k 's corresponding to \uparrow ($l = 0, \pm 3$) and \downarrow ($k = \pm 1, \pm 2$) respectively. The first order energy corrections will be shown to reasonably describe the MBL phase. Based on this perturbative form of the QCTF, the entanglement measure is obtained using relation (9) as follows:

Appendix E1 for further explanation). As a result, the most significant (lowest perturbation order) non-zero frequency contributions correspond to $l = 0$ and $k = \pm 1$,

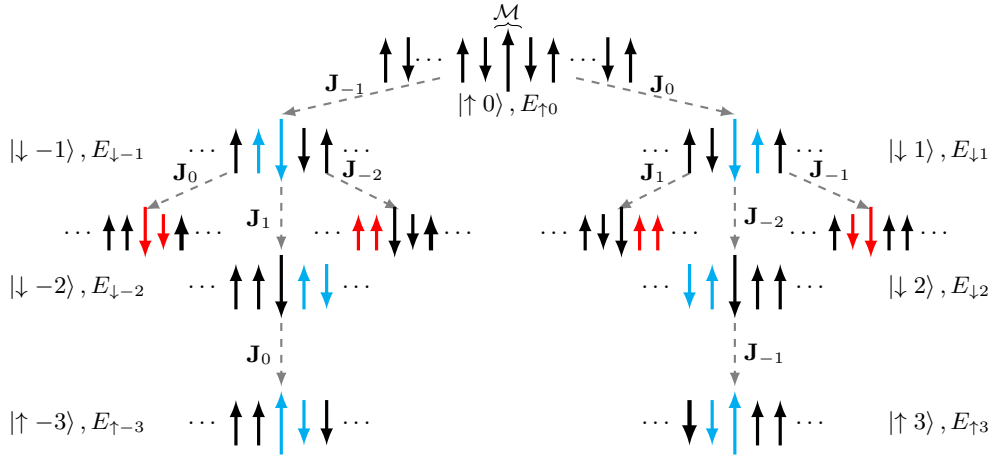


FIG. 2. Network illustration of interference between unperturbed (product) eigenstates due to local exchange interactions, for a spin in the chain's bulk. This figure shows how the unperturbed states ($|\uparrow \text{ or } \downarrow\rangle_{\mathcal{M}} \otimes |l\rangle$), interfere locally to produce the exact eigenstates of the spin chain during the perturbation process. The spin \mathcal{M} , for which we study its entanglement dynamics, is drawn slightly taller. The ket notation and zeroth order energy of each chain are denoted adjacently. The local interaction Hamiltonians $\mathbf{J}_k = J\mathbf{S}_k\mathbf{S}_{k+1}$, written on the vertices, flips anti-parallel spins (k and $k+1$), and leaves the parallel spins unchanged. Upon applying the perturbations at each step, the flipped spins are colored in blue, and the unchanged ones are colored in red. Since the initial state of the chain is the anti-ferromagnetic state ($|\uparrow 0\rangle$), the number of vertices linking this state to another state in this figure, indicates the order of perturbations required to relate these two states. Note that, although a few of the spins are illustrated, the spin chain can be arbitrarily long. In this figure, we show all of the significant (up to the third order of perturbation) interferences caused by the interaction Hamiltonian (\mathbf{J}). This figure also demonstrates that in a spin chain with nearest-neighbor interactions, a spin at the distance n is connected to the chosen spin (\mathcal{M}) via at least n local perturbation steps; here, connected means that the spin is flipped via a series of local perturbations, initiated from \mathcal{M} . This observation is further used in the subsection IV B to show the exponential decay of quantum correlation between spins in the MBL phase.

which are the second order contributions to $\tilde{Q}_{\mathcal{M}}(s)$ at frequencies $f = \pm|E_0^{(1)} - E_{\pm 1}^{(1)}|/\hbar$, such that

$$\begin{aligned} \tilde{Q}_{\mathcal{M}}^{(2)}(s) &= c_{\pm 10}c_{0\pm 1}\left(s + \frac{i}{\hbar}(E_0^{(1)} - E_{\pm 1}^{(1)})\right)^{-1} \\ &+ c_{\pm 10}^*c_{0\pm 1}^*\left(s + \frac{i}{\hbar}(E_{\pm 1}^{(1)} - E_0^{(1)})\right)^{-1}, \end{aligned} \quad (18)$$

where $\tilde{Q}_{\mathcal{M}}^{(2n)}(s)$ denotes the contributions of order $2n$ to the entanglement measure. According to this relation, the location of second-order frequencies (f) and their corresponding amplitudes ($a \doteq 2|c_{\pm 10}|^2$) can be obtained in terms of probability density functions, denoted by $P_F^{(2)}(f)$ and $P_A^{(2)}(a)$ respectively. If $P_h(x)$ denotes the uniform distribution of h_i 's on the interval $[-W, W]$, we can show that (see Appendix E 2 and E 3 for the proof)

$$\begin{aligned} P_F^{(2)}(f) &= \begin{cases} \hbar\left(\frac{1}{W} - \frac{J}{2W^2}\right) & 0 \leq f \leq \frac{J}{\hbar}, \\ \hbar\left(\frac{1}{W} - \frac{f}{2W^2}\right) & \frac{J}{\hbar} < f \leq \frac{2W-J}{\hbar}, \\ \hbar\left(\frac{J+2W-f}{4W^2}\right) & \frac{2W-J}{\hbar} < f \leq \frac{2W+J}{\hbar}, \\ 0 & \text{otherwise.} \end{cases} \quad (19) \\ P_A^{(2)}(a) &\approx \begin{cases} \frac{J \ll W}{W} - \frac{\hbar f}{2W^2}; & 0 \leq f \leq \frac{2W}{\hbar}, \\ \frac{W}{8\left(\frac{W}{J}a\right)^2}; & a \geq \frac{1}{8}\left(\frac{J}{W}\right)^2, \end{cases} \quad (20) \end{aligned}$$

which are shown in Figure 3. According to (20), the

second-order frequency amplitude is lower bounded at $a_0 = \frac{1}{8}\left(\frac{J}{W}\right)^2$. This value provides a lower bound on the entanglement amplitude in the MBL phase to second order perturbation theory, which is expected to adequately predict the entanglement dynamics, as explained in the next subsection.

Despite the adequacy of second order perturbation theory, it is important to assess the (next) fourth order contributions. The fourth-order contributions appear for a collective variety of indices in the summations, in (17); for instance $l = 0 (i = -1, i' = 0)$ with $k = 1 (j = 1, j' = 0)$ produces $(E_{-1}^{(1)} - E_1^{(1)})/\hbar$. Non-zero frequencies which appear as fourth-order contributions are $\pm|E_{-1}^{(1)} - E_1^{(1)}|/\hbar$, $\pm|2E_0^{(1)} - E_{\pm 1}^{(1)} - E_{\mp 1}^{(1)}|/\hbar$, $|E_{\pm 2}^{(1)} - E_0^{(1)}|/\hbar$, $\pm 2|E_{\pm 1}^{(1)} - E_0^{(1)}|/\hbar$ and $\pm|E_{\pm 1}^{(1)} - E_0^{(1)}|/\hbar$. The latter set of frequencies is identical to the second-order frequency components. Interference to $|\pm 3\rangle$ appears in the sixth-order contributions, for instance $l = 0 (i = 0, i' = 0)$ with $k = 3 (j = 3, j' = 0)$ produces the frequency $(E_0^{(1)} - E_3^{(1)})/\hbar$.

Thus, the spin's entanglement measure was obtained from the system's perturbed form of QCTF, which includes the contributing frequency components sorted by their corresponding perturbation order. Here, we can take advantage of this analysis to clarify the main idea of QCTF, which is to obtain the entanglement dynamics directly from the system's Hamiltonian properties with-

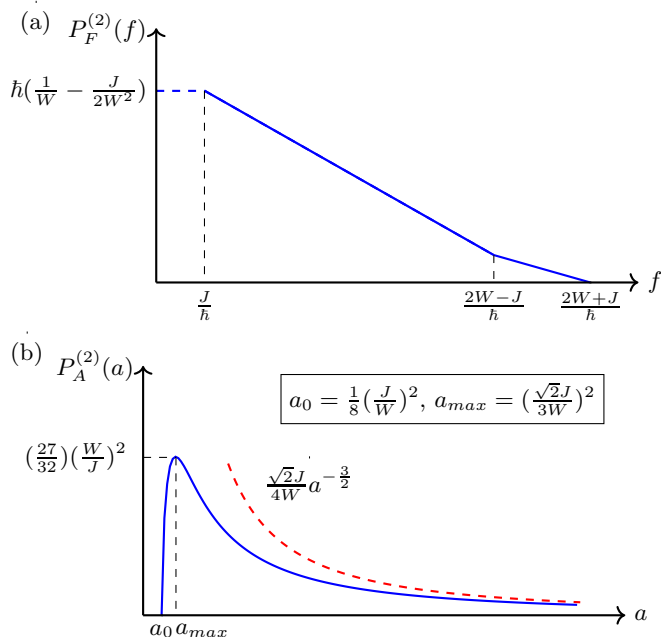


FIG. 3. Illustration of the PDFs for (a) the frequency components and (b) their amplitudes in the lowest (second) order perturbation of the entanglement measure $\tilde{Q}_{\mathcal{M}}^{(2)}(s)$ for a spin in the bulk of the chain. Sub-figure (a) shows the PDF for the second order frequencies $P_F^{(2)}(f)$ in (19). These frequencies most significantly contribute to the entanglement measure of the spin \mathcal{M} . For frequencies close to and smaller than $\frac{J}{h}$ (plotted with a dashed line), the local energy levels are vulnerable to strong mixing with the other energy levels (corresponding to the neighboring sites), which interferes with the perturbative treatment; but, the probability of this subset of frequencies contributing is approximately J/W , which is negligibly small in the MBL phase ($J \ll W$). Sub-figure (b) shows the PDF for second order amplitudes, $P_A^{(2)}(a)$. In the MBL phase, small amplitudes (i.e., on the order of $(\frac{J}{W})^2$) are highly probable, with a lower cut-off at a_0 . As shown in this sub-figure, the most probable amplitude (a_{max}) is located very close to the lower cut-off frequency, when taking into account the slow convergence of this PDF at high amplitudes (i.e., scaling as $a^{-\frac{3}{2}}$, plotted as a red dashed line). The lower cut-off implies the existence of a minimum amplitude in the entanglement measure in the MBL phase.

out evaluating the system's time evolution. Although at first glance, the QCTF (16) transforms the entire off-diagonal block in the system's density matrix, this transformation as well as the dynamical measure (17) specify the *structure* of the terms in the density matrix and in the entanglement dynamics, respectively. Each frequency component in (18) specifies the *relative* phase, and its corresponding amplitude, between the terms in the density matrix that contribute to the entanglement measure. This description is made possible through the \star operation. For instance, in the second-order entanglement measure (18) the relative frequency components are highly simplified. This procedure allows for avoid-

ing the detailed calculation of the (many-body quantum system's) time-evolution and instead evaluating specific amplitudes and frequencies in the entanglement measure. In the next subsection, we prove that the contributions of the frequency components diminish as the perturbation order increases.

B. Exponential attenuation of high order perturbation amplitudes

In this subsection, we show that although the number of frequency components in the entanglement measure increases with the order of perturbation, their contribution gets exponentially suppressed. This property, not only validates the convergence of perturbation series (17), more importantly, it captures the essence of the MBL dynamics, as will be discussed. According to (17) and the definition of the c_{ij} 's, the amplitudes of the $2n$ th-order contributions scale as $J^{2n} ((h_{i_1} - h_{i_2})(h_{i_3} - h_{i_4}) \cdots (h_{i_{4n-1}} - h_{i_{4n}}))^{-1}$ where indices can be repeated, e.g., $i_2 = i_3$. Here, the scaling property of these random amplitudes is analyzed. This goal can be achieved by finding their PDFs, which is similar to finding $P_A^{(2)}(a)$ for the case of $2n = 2$ in the last subsection. Nevertheless, obtaining the PDFs is not a straight-forward way to assess the contribution of the frequency components, because it provides unnecessary detail about their amplitudes. Instead, the critical probability $\mathbf{P}^{(2n)} \doteq \mathbf{P}\{J^{2n} |(h_{i_1} - h_{i_2})(h_{i_3} - h_{i_4}) \cdots (h_{i_{4n-1}} - h_{i_{4n}})|^{-1} > 1\}$ can be studied. This probability is an indicator of the rate of convergence for the multi-variable perturbation series (17). In the MBL phase, the probability for $|h_i - h_j| < J$ is approximately J/W (refer to Appendix E 2 for detail). Although this property does not directly imply that $\mathbf{P}^{(2n)}$ scales exponentially in the order number ($\sim (J/W)^{2n}$), by employing the Mellin transformation [49] we show that this property indeed holds.

In our analysis, we use the approximation that the probability densities for terms $|J/(h_i - h_j)| \sim P_A^{(1)}(a)$ are independent, i.e., we ignore the repeated indices. This approximation not only simplifies the analysis enabled by the use of the Mellin transformation, it is also physically relevant, that is, in the $W \gg J$ limit, taking into account the repeated indices decreases the critical probability, therefore, this approximation gives an upper bound for $\mathbf{P}^{(2n)}$ (refer to Appendix F for more details). Importantly, through this approximation, we are also generalizing the results to initial states beyond the anti-ferromagnetic order. More precisely, as inferred from Figure 2, the initial state of the system prescribes how the indices should be repeated, therefore, by considering independent PDFs, we obtain an upper-bound for the critical probability that reflects a wider range of initial states (all of the unperturbed Hamiltonian's eigenstates).

The critical probability can be written in terms of the

PDF $\hat{P}^{(2n)}(x)$ for $|\frac{h_{i_1}-h_{i_2}}{J} \dots \frac{h_{i_{4n-1}}-h_{i_{4n}}}{J}|$ as follows,

$$\begin{aligned} \mathbf{P}^{(2n)} &= \mathbf{P}\left\{ \left| \frac{h_{i_1}-h_{i_2}}{J} \dots \frac{h_{i_{4n-1}}-h_{i_{4n}}}{J} \right| \leq 1 \right\} \\ &= \int_0^1 \hat{P}^{(2n)}(x) dx. \end{aligned} \quad (21)$$

In Appendix F we obtain the PDF $\hat{P}^{(2n)}(x)$ and show that

$$\begin{aligned} \ln(\mathbf{P}^{(2n)}) &\approx 2n \ln\left(\frac{J}{W}\right) \\ &+ (2n-1) \left(\ln\left(\frac{2n \ln\left(\frac{2W}{J}\right)}{2n-1}\right) + 1 \right) \\ &\approx 2n \left(\ln\left(\frac{2n \frac{J}{W} \ln\left(\frac{2W}{J}\right)}{2n-1}\right) \right), \end{aligned} \quad (22)$$

which is approximately linear in $2n$ within an acceptable approximation ($\frac{2n}{2n-1} \approx 1$ for large n). Also, this formula gives the decay rate, which is approximately $\frac{J}{W} \ln \frac{2W}{J}$, for spins located further than the immediate neighbouring sites. Thus, the critical probability $\mathbf{P}^{(2n)}$, which is an indicator of the rate of convergence in the multi-variable perturbation series (17), decays exponentially with the order of perturbation. *Therefore, in the MBL phase, the few contributing second-order frequencies are exponentially dominant.* Furthermore, the exponential dominance of (non-zero) second-order frequency components supports the absence of DC transport in the MBL phase, which was conjectured to hold [37].

It is important to note that this analysis is not limited to disordered Heisenberg spin chains. Although generalizing this result to all disordered spin chains is beyond the scope of this paper and requires a detailed analysis, the theoretically demonstrated *exponential dominance of low-order collaborating frequencies in the entanglement measure leads to suppressed, and quasi-periodic entanglement dynamics (after a quench to an strongly-interacting Hamiltonian) when the system is initially at one of the eigenstates of its un-perturbed (disordered) Hamiltonian. This behavior is the essence of MBL dynamics.*

C. Numerical illustration and validation of the QCTF approach to MBL

The theoretical analysis in Subsections IV A-IV B is illustrated and verified here by exact numerical simulations. Figure 4 shows the dynamical entanglement measure in the frequency domain for three spins in a disordered ($\frac{W}{J} = 10$) Heisenberg chain of fifteen spins, evolving unitarily according to the Hamiltonian (13) from an anti-ferromagnetic state. To this end, upon obtaining the entanglement measures, $\mathcal{Q}_{\mathcal{M}}(t)$, which are not shown here for brevity, their corresponding Fourier transforms, $(\mathcal{F}\{\mathcal{Q}_{\mathcal{M}}(t)\})$, are compared with the predictions of the

QCTF approach, given in sub-section IV A. More precisely, the QCTF approach predicts the singularities in $\tilde{\mathcal{Q}}_{\mathcal{M}}(s)$ (for instance, the second-order poles are given in (18)), shown using black lines in Figure 4. Because the poles are purely imaginary, they coincide with the peaks in the numerically obtained Fourier spectra. The quasi-periodicity of the entanglement measures is confirmed by the observation of a few (one for the edge spin, and two for bulk spins) dominant non-zero frequency components in their corresponding Fourier transformations. The small deviations between the predicted and observed frequencies are due to both the error in the Fourier transformation (due to the finite simulation time) and the (neglected) higher-order perturbations to the energy values. This particular realization of the disordered Heisenberg chain, in addition to demonstrating the effectiveness of the QCTF approach, shows different avenues from which higher order effects can interfere with the second-order approximation of the entanglement dynamics, as discussed in the caption of Figure 4.

To test our results in more depth, we numerically iterate the unitary evolution of 10^6 random realizations of the disordered Heisenberg spin chain (13) with $J = 1$ and $W = 10, 15$ and 20 from an anti-ferromagnetic state. Followed by evaluating the system's state, we obtain the density matrix for spins at the edge and in the bulk (with at least two sites away from the edges) of chains with six spins. As discussed in the previous subsection and demonstrated in Figure 4, the second-order frequency components correspond to interactions with immediate neighbours, which also make up the major part of the spin's entanglement dynamics. Therefore, by considering smaller chains here, the statistics of the second-order frequencies is not affected and access to a higher number of simulation samples (10^6) is made computationally feasible. Eventually, we reconstruct the PDFs $P_F^{(2)}(f)$ and $P_A^{(2)}(a)$ through extracting the peaks in the Fourier transformation (at the locations predicted by our analysis) of the entanglement measure, as shown in Figure 5. The numerical results confirm the QCTF theoretical predictions at all of the disorder strengths, with higher precision at stronger disorders, as expected. Due to the difference in first-order energy corrections for an edge spin compared with a spin in the bulk of the chain, the PDFs of the second-order frequencies are slightly different, particularly at the high-frequency corner of the PDFs (refer to Appendix E3 for more detail). This phenomenon is captured in the numerical simulation, as shown in the insets in Figure 5(a), which affirms the effectiveness of the QCTF perturbative analysis. The deviation between the numerical and theoretical PDFs, which results from higher order contributions, fades away as the disorder strength increases, as shown in Figure 5(b).

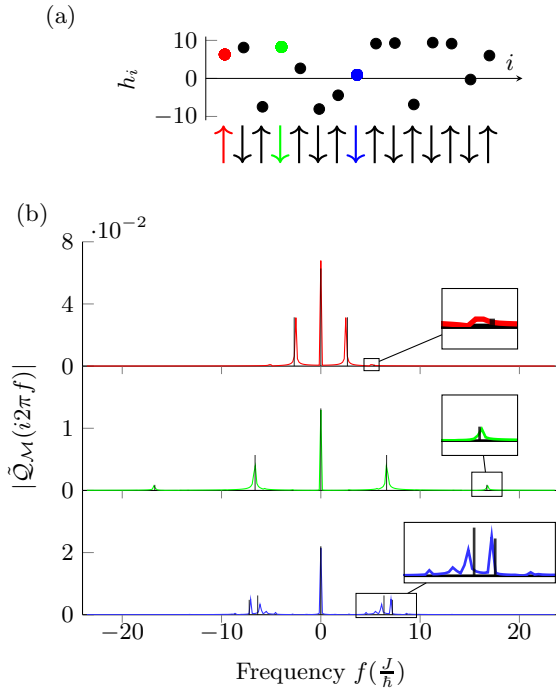


FIG. 4. This figure shows the quenched entanglement measure in the frequency domain $|\hat{Q}_{\mathcal{M}}(s = i2\pi f)|$ for three particles in a disordered ($W = 10$) Heisenberg chain of fifteen spins, initialized at an anti-ferromagnetic state. The random fields h_i and the location of the three particular spins are shown in sub figure (a) in red (first spin from left), green (fourth spin) and blue (spin in the middle of the chain). The Fourier transforms of the corresponding entanglement measures for each particle from a $40\frac{\hbar}{J}$ -long exact numerical simulation are shown in sub figure (b) in the same colors. The black lines show the predicted dominant frequency components in the entanglement measure from the QCTF analysis. Note that all of the non-zero frequencies appear in positive and negative pairs. Smaller peaks have been magnified in the insets. As shown in the top plot in sub figure (b), the entanglement measure for the edge spin has only one dominant (non-zero) frequency pair, accompanied by a fourth order pair of frequency components at $\pm 2|E_{\pm 1}^{(1)} - E_0^{(1)}|/\hbar$ (shown in the inset). The second plot, corresponding to the fourth spin, shows two non-zero dominant pairs of frequency components. In the bottom plot, which corresponds to the spin in the middle of the chain (blue), fourth order components are present, although their contribution is small. The main reason for this behavior is that $|h_{10} - h_9|/J \ll 1$ which strongly reinforces higher order interferences for particles 9 and 8. The frequency spectra are dominated by the few second-order frequency components, which are predicted by the QCTF formulation. This property ultimately leads to quasi-periodicity of the entanglement measures.

V. CONCLUSION

The new description of quantum many-body dynamics through QCTF provides an equivalent representation as the wave-function or the density matrix formalisms,

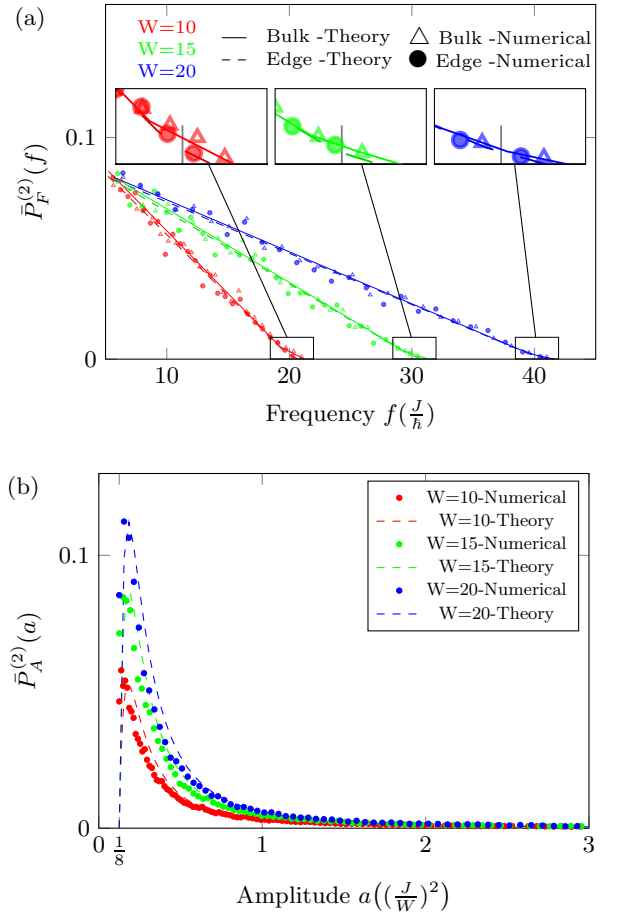


FIG. 5. Numerically constructed PDFs $P_F^{(2)}(f)$ and $P_A^{(2)}(a)$ compared with QCTF theoretical predictions. This figure shows the discretized PDFs for second-order frequencies and amplitudes. Note that due to the numerical discretization, vertical axes, which are denoted by $\bar{P}_F^{(2)}(f)$ and $\bar{P}_A^{(2)}(a)$, are scaled (by a function of the (adaptive) length of the bins). In this simulation, the coupling and disorder strengths are $J = 1$, $W = 10, 15$ and 20 . Sub-figure (a) shows the re-constructed $\bar{P}_F^{(2)}(f)$, for spins at the edges and in the bulk of the chain. The insets show the details of these PDFs at their high-frequency corners, where the edge spins are expected to behave differently than the bulk spins due to their differing first-order energy correction (see Appendix E 2 for more detail). As expected, the different statistics between these two classes of spin subsystems is more noticeable at the lowest disorder strength ($W = 10$). With the help of a large number of random samples (10^6), this difference is captured. The numerical PDF is constructed based on the frequency samples larger than $5\frac{J}{\hbar}$ to avoid unlikely regions in the chain with strong mixing affects, as explained in Figure 3. Sub-figure (b) shows the re-constructed $\bar{P}_A^{(2)}(a)$. The precision of the theoretical prediction generally increases with the disorder strength; In particular, the features match accurately near the sharp peaks. The deviation between the numerical PDFs and their respective theoretical predictions at low disorder strengths are due to the fourth-order contributions, which smoothly fade away at higher disorder strengths. Also, note that as a result of the very sharp increase of the PDFs near their lower cut-off, it is numerically infeasible to fully capture the statistics at these amplitudes with even a high number of simulations.

while explicitly revealing the correlation dynamics in the system. This new formalism allows for obtaining the entanglement dynamics in a quantum system *directly* from the system's Hamiltonian features, therefore it circumvents the bottleneck of evaluation of many-body system's evolution. As a result, a measure for the entanglement dynamics of two-energy level particles of a many-body quantum system was obtained through integrating the QCTF along specific closed contours. The QCTF treatment was shown to be capable of efficiently characterizing the entanglement of highly-correlated many-body eigenstates, which provides a theoretical framework for further studying the Eigenstate Thermalization Hypothesis (ETH).

In addition to the general QCTF formulation presented in this paper, a primary application focus was on the MBL dynamics in the disordered Heisenberg spin chains, for which the spin's entanglement dynamics were characterized in terms of probability density functions for amplitudes and corresponding frequency components of the entanglement measure. The QCTF method allowed for implementing time-independent perturbation theory to directly obtain the particle's entanglement, while bypassing the evaluation of system's time evolution. This capability enabled us to prove a critical conjecture regarding the MBL phase that the entanglement's dynamics is dominated by local interactions and the effect of further sites decays exponentially [41–43]. Accordingly, we showed that entanglement's evolution of a spin in the chain's bulk is quasi-periodic in time. This finding supports the absence of DC transport in the MBL phase, which was also conjectured to hold in strongly-interacting chains [12, 37], and had been shown to exist in weakly-interacting spin chains [50]. Furthermore, in this analysis we obtained the minimum possible amplitude for the dominant frequency components of the subsystem's entanglement, which implies a lower bound on the quasi-periodic entanglement amplitude in the MBL phase. The QCTF analysis can be applied to different probability distributions for the disordered field, which we denoted by $P_h(x)$, e.g., a Gaussian field, which shows one aspect of the generality of the QCTF formulation.

Although the principles and the basic form of QCTF are defined in general, that includes treating mixed quantum states, the application of QCTF in the paper was focused on entanglement dynamics of pure state quantum systems. This special focus was motivated by recent experimental observations and theoretical arguments on quantum thermalization and MBL in *isolated* pure state quantum systems.

The QCTF approach was employed in two different ways: exact, when quantifying the static entanglement of

many-body eigenstates in Section III and perturbative, in the MBL analysis in Section IV. Although employing the general QCTF formulation is not limited to these two means of utilization, other ways that QCTF can be employed will be a subject for future research. Additionally, there are several directions for future research building on the QCTF formalism. One application is to consider the MBL phenomenon in different spin- $\frac{1}{2}$ lattice geometries, e.g., 2D spin networks or the effect of long-range interactions on the MBL dynamics. Another direction is to extend the entanglement analysis to mixed quantum states and to systems where the particles each have a higher number of energy levels. Furthermore, based on the equivalence of the QCTF and density matrix descriptions, other classes of quantum phenomena, such as high-order correlations [22] and multi-partite entanglement [51] can be studied by linking the Hilbert space basis vectors to the real space (lattice) coordinates. Additionally, the QCTF framework should be considered to address quantum systems with time-dependant Hamiltonians, including the important class of controlled quantum systems. In this regard, the QCTF approach has the prospect of providing a new theoretical framework to control entanglement dynamics in many-body quantum systems, which is of significant importance to potentially many applications including quantum information science. In summary, we hope that the QCTF provides a means to analyze many-body quantum statistical mechanics, that yields new insights of fundamental and practical significance.

ACKNOWLEDGMENTS

P.A acknowledges support from the U.S Department Of Energy (DOE) grant (DE-FG02-02ER15344) and the Princeton Program in Plasma Science and Technology (PPST). H.R acknowledges support from the Army Research Office (ARO) grant (W911NF-19-0382).

APPENDIX

The Appendices contain detailed proofs and derivations of several items stated in the main text.

Appendix A: Derivation of equation (3)

Using equation (1), we can rewrite the R.H.S of equation (3) as follows

$$\frac{1}{(2\pi i)^3} \oint_{\partial C_s} ds \oint_{\partial C_d} dz_d \oint_{\partial C_a} dz_a e^{st'} \sum_{l,k} \sum_{l'',k''} \langle k|k' \rangle \langle l'|l \rangle z_d^{(l''-k'')-(l-k)-1} z_a^{(l''+k'')-(l+k)-1} \langle l''|\tilde{\rho}(s)|k'' \rangle. \quad (\text{A1})$$

Note that the three integrals are independent and can be evaluated interchangeably. We consider the z_d and z_a integrals first. Using the fact that the integrand is holomorphic inside the closed contours ∂C_d and ∂C_a , except at the origin, by employing Cauchy's residue theorem the value of these two integrations are equal to the residue of the integrand at the origin ($z_d = 0, z_a = 0$) times

$$(3) = \frac{1}{2\pi i} \oint_{\partial C_s} ds e^{st'} \sum_{l,k} \langle l'|l \rangle \langle l|\tilde{\rho}(s)|k \rangle \langle k|k' \rangle = \langle l'|\frac{1}{2\pi i} \oint_{\partial C_s} ds e^{st'} \tilde{\rho}(s)|k' \rangle = \langle l'|\rho(t')|k' \rangle, \quad (A2)$$

where we have used the definition of the inverse Laplace transform, and the linearity of the transform.

Appendix B: Derivation of equation (5)

Here, we show that the QCTF in (5) can be interpreted as a transformation of the system's density matrix using one chronological frequency, s , and two structural

frequencies, z_a and z_d . Using (4) and the definition of operation \star , we can rewrite (5) as

$$\begin{aligned} \mathcal{K}(z_d, z_a, s) &\doteq \bar{\mathcal{K}}(z_d z_a, s) \star \bar{\mathcal{K}}^*((z_a/z_d)^*, s^*) \\ &= \sum_{l,k=0}^{d-1} \langle l|\mathbf{G}(s)|\psi_0 \rangle \star \langle \psi_0|\mathbf{G}^\dagger(s^*)|k \rangle z_d^{l-k} z_a^{l+k}. \end{aligned} \quad (B1)$$

We define $\tilde{c}_l(s) \doteq \langle l|\mathbf{G}(s)|\psi_0 \rangle = \mathcal{L}\{\langle l|\psi(t)\rangle\} = \mathcal{L}\{c_l(t)\}$. Then using definition (6) results in:

$$\begin{aligned} \tilde{c}_l(s) \star \tilde{c}_k^*(s^*) &= \frac{1}{2\pi i} \int_{-\infty}^{\infty} d\omega \tilde{c}_l(\sigma + i\omega) \tilde{c}_k^*((s - \sigma - i\omega)^*) \\ &= \int_{-\infty}^{\infty} dt_1 \int_{-\infty}^{\infty} dt_2 \frac{1}{2\pi i} \int_{-\infty}^{\infty} d\omega c_l(t_1) c_k^*(t_2) e^{-st_2 - \sigma(t_1 - t_2) - i\omega(t_1 - t_2)} \\ &= \int_{-\infty}^{\infty} dt_1 \int_{-\infty}^{\infty} dt_2 c_l(t_1) c_k^*(t_2) e^{-st_2 - \sigma(t_1 - t_2)} \delta(t_1 - t_2) \\ &= \int_{-\infty}^{\infty} dt c_l(t) c_k^*(t) e^{-st} = \langle l|\tilde{\rho}(s)|k \rangle. \end{aligned} \quad (B2)$$

Therefore, substituting $\langle l|\mathbf{G}(s)|\psi_0 \rangle \star \langle \psi_0|\mathbf{G}^\dagger(s^*)|k \rangle$ in (B1) with $\langle l|\tilde{\rho}(s)|k \rangle$ gives:

$$\mathcal{K}(z_d, z_a, s) = \sum_{l,k=0}^{d-1} \langle l|\tilde{\rho}(s)|k \rangle z_d^{l-k} z_a^{l+k}. \quad (B3)$$

Appendix C: Proof of equation (9)

We start from the system's state in the time domain, $|\psi(t)\rangle$, and expand it in the product basis vectors of each subsystem, $\{|+\rangle, |-\rangle\}$, and $\{|l\rangle, l = 0, \dots, d-1\}$, as follows

$$\begin{aligned} |\psi(t)\rangle &= \sum_{a \in \{+, -\}} \sum_{l=0, \dots, d-1} c_{al}(t) |a \otimes l\rangle; \\ c_{al}(t) &= \langle a \otimes l|\psi(t)\rangle. \end{aligned} \quad (C1)$$

Based on this expansion, we may construct the matrix $M_{2 \times d}$ such that its first and second rows consist of $\{c_{+l}(t)\}$ and $\{c_{-l}(t)\}$ respectively (the time dependence in c 's are not shown below for simplicity):

$$M(t) \doteq \begin{pmatrix} c_{+0} & c_{+1} & \cdots & c_{+l} & \cdots & c_{+d-1} \\ c_{-0} & c_{-1} & \cdots & c_{-l} & \cdots & c_{-d-1} \end{pmatrix}. \quad (C2)$$

If subsystem \mathcal{M} is not entangled to subsystem \mathcal{R} at $t = t'$, then $|\psi(t')\rangle$ is a product state and the rows of $M(t')$ are linearly dependent, i.e. $\text{rank}(M(t')) = 1$. This condition on the rank of M is necessary and sufficient for the subsystem \mathcal{M} to not be entangled to subsystem \mathcal{R} . Thus, if $\text{rank}(M) = 2$ these subsystems are entangled. To construct a smooth indicator of entanglement, consider the following square sub-matrices $M_{2 \times 2}^{ij}$, formed from the i th and j th columns of M ,

$$M^{ij}(t) \doteq \begin{pmatrix} c_{+i} & c_{+j} \\ c_{-i} & c_{-j} \end{pmatrix}, \quad (C3)$$

and use them to define the entanglement measure $\mathcal{Q}_{\mathcal{M}}(t)$ as follows:

$$\mathcal{Q}_{\mathcal{M}}(t) \doteq \sum_{0 \leq i < j \leq d-1} |\det(M^{ij}(t))|^2. \quad (\text{C4})$$

More generally, $\mathcal{Q}_{\mathcal{M}}(t') = 0$ is a necessary and sufficient condition for the subsystem \mathcal{M} not to be entangled at t' .

Expanding the summations in $\mathcal{Q}(M)$ will result in

$$\mathcal{Q}_{\mathcal{M}}(t) = \sum_{0 \leq i < j \leq d-1} \det(M^{ij})(\det(M^{ij}))^* \quad (\text{C5a})$$

$$= \sum_{0 \leq i < j \leq d-1} (c_{+i}c_{-j} - c_{+j}c_{-i})(c_{+i}^*c_{-j}^* - c_{+j}^*c_{-i}^*)$$

$$= \sum_{0 \leq i \neq j \leq d-1} |c_{+i}|^2|c_{-j}|^2 - \sum_{0 \leq i \neq j \leq d-1} c_{+i}c_{-j}c_{+j}^*c_{-i}^*$$

$$= \sum_{0 \leq i, j \leq d-1} |c_{+i}|^2|c_{-j}|^2 - \sum_{0 \leq i, j \leq d-1} c_{+i}c_{-j}c_{+j}^*c_{-i}^*$$

$$= \left(\sum_{0 \leq i \leq d-1} |c_{+i}|^2 \right) \left(\sum_{0 \leq i \leq d-1} |c_{-i}|^2 \right) \quad (\text{C5b})$$

$$- \left(\sum_{0 \leq i \leq d-1} c_{+i}c_{-i}^* \right) \left(\sum_{0 \leq i \leq d-1} c_{+i}^*c_{-i} \right) \quad (\text{C5c})$$

$$= \left| \frac{\sum_i |c_{+i}|^2}{\sum_i (c_{+i}^*c_{-i})} \frac{\sum_i (c_{+i}c_{-i}^*)}{\sum_i |c_{-i}|^2} \right| = \det(\rho_{\mathcal{M}}(t)),$$

which is the determinant of the time dependent reduced density matrix of subsystem \mathcal{M} .

As the second step, here we prove that the R.H.S of equation (9) is the Laplace transform of $\mathcal{Q}_{\mathcal{M}}(t)$. We start from the first term in (9). Before proceeding, we introduce the notation $\tilde{c}_{al}(s) \doteq \mathcal{L}\{c_{al}(t)\} = \langle a \otimes l | \mathbf{G}(s) | \psi_0 \rangle$. Therefore, by using the definition of $\mathcal{K}(z_a, z_d, s)$ in (8b), the first term in (9) and the fact that the \star operation is associative and commutative, we have

$$(2\pi i)^{-2} \sum_{l,k} \sum_{l',k'} \oint_{\partial C_d} \mathbf{d}z_d \oint_{\partial C_a} \mathbf{d}z_a \tilde{c}_{+l}(s) \star \tilde{c}_{-k}^*(s^*) \star \tilde{c}_{+l'}^*(s^*) \star \tilde{c}_{-k'}(s) z_a^{l+k-l'-k'-1} z_d^{l-k+k'-l'-1}. \quad (\text{C6})$$

Upon employing Cauchy's residue theorem, based on the definition of the closed contours ∂C_d and ∂C_a , then the value of the double integral is equal to $(2\pi i)^2$ times the residue of the integrand at the origin of the structural space (z_d, z_a) , which is the coefficient of $z_d^{-1}z_a^{-1}$ in the double summation. Therefore, the only remaining terms after the double integration must satisfy the following set

of conditions:

$$\begin{cases} l+k-l'-k'-1 = -1 \\ l-k+k'-l'-1 = -1 \end{cases} \iff \begin{cases} l=l' \\ k=k' \end{cases}. \quad (\text{C7})$$

Consequently, the first term in (9) is:

$$\sum_{l,k} \tilde{c}_{+l}(s) \star \tilde{c}_{+l}^*(s^*) \star \tilde{c}_{-k}(s) \star \tilde{c}_{-k}^*(s^*) = \mathcal{L}\left\{ \sum_{l,k} |c_{+l}|^2 |c_{-k}|^2 \right\}, \quad (\text{C8})$$

which is the Laplace-dual of (C5b). In the last step, we operated with \star similar to our calculation in equation (B2). Based on this equality, by showing that the second term in (9) corresponds to (C5c), the proof is accomplished. To this end, we first consider $\mathcal{K}_d(z_a, s)$. Based

on the definitions (8b) and (9) we have:

$$\mathcal{K}_d(z_a, s) = (2\pi i)^{-1} \sum_{l,k} \oint_{\partial C_d} \mathbf{d}z_d \tilde{c}_{+l}(s) \star \tilde{c}_{-k}^*(s^*) z_a^{l+k} z_d^{l-k-1}. \quad (\text{C9})$$

Applying the Cauchy's residue theorem, the integral is equal to $(2\pi i)$ times the residue of the integrand at the

origin of the z_d space, which is the coefficient of z_d^{-1} in its Maclaurin expansion. Therefore, it is easy to see that for this integrand, only the terms with $l = k$ remain after the integration and we have

$$\mathcal{K}_d(z_a, s) = \sum_l \tilde{c}_{+l}(s) \star \tilde{c}_{-l}^*(s^*) z_a^{2l}. \quad (\text{C10})$$

$$\sum_{l,k} \tilde{c}_{+l}(s) \star \tilde{c}_{-l}^*(s^*) \star \tilde{c}_{+k}^*(s^*) \star \tilde{c}_{-k}(s) z_a^{2(l-k)} \Big|_{z_a=1} = \mathcal{L} \left\{ \sum_{l,k} c_{+l} c_{-k} c_{+k}^* c_{-l}^* \right\}, \quad (\text{C11})$$

which is the Laplace-dual of the second term in (C5c). Therefore, using the linearity of the Laplace transformation, the R.H.S of (9) is equal to the Laplace transformation of $\mathcal{Q}_{\mathcal{M}}(t)$, which proves the assertion (9).

Appendix D: Locality/non-locality of the eigenstate $|A\rangle$

Here we demonstrate how $|\langle A^+ | A^- \rangle|$ is a measure of non-locality of the eigenstate $|A\rangle$ at the location of subsystem \mathcal{M} . By expanding $|A^-\rangle$ in the new set of basis kets ($\{|\tilde{l}\rangle\}$), (10) can be rewritten as

$$|A\rangle = (\alpha^+ |+\rangle + \alpha^- \langle A^+ | A^- \rangle |-\rangle) \otimes |A^+\rangle + \alpha^- |-\rangle \otimes \sum_{\tilde{l} \neq 0} \langle \tilde{l} | A^- \rangle |\tilde{l}\rangle. \quad (\text{D1})$$

Therefore, if $|\langle A^- | A^+ \rangle| \approx 1$ then $|A\rangle \approx (\alpha^+ |+\rangle + \alpha^- e^{\arg(\langle A^+ | A^- \rangle)} |-\rangle) \otimes |A^+\rangle$ is very similar to a product state (i.e., it has local character). On the other hand, $|\langle A^- | A^+ \rangle| \approx 0$ implies that $|A\rangle \approx \alpha^+ |+\rangle \otimes |A^+\rangle + \alpha^- |-\rangle \otimes \sum_{\tilde{l} \neq 0} \langle \tilde{l} | A^- \rangle |\tilde{l}\rangle$, which is strictly non-local at the position of \mathcal{M} .

Appendix E: Mathematical details of section IV

1. Minimum perturbation order in (17)

For specific values of l and k in the outer summation in (17), we first consider the inner summation over i , for which there is a term of the form $c_{i0}^* c_{il}$. Due to (15), the order of perturbation for such a term is $|i| + |i - l|$, which has its smallest value equal to $|l|$, when $0 \leq i \leq l$ or $l \leq i \leq 0$. The same argument holds for each of the other indices j, i' and j' ; therefore, for a particular set of l and k , the smallest order of perturbation is $2(|l| + |k|)$.

Consequently, the second term in (9) is

2. Derivation of $P_F^{(2)}(f)$

In general, if the disorder coefficients (h_i) are drawn randomly from the PDF $P_h(x)$, denoted by $h_i \sim P_h(x)$, then we have:

$$E_{\uparrow 0} - E_{\downarrow \pm 1} = E_0^{(1)} - E_{\pm 1}^{(1)} + \langle \mathbf{J} \rangle_0 - \langle \mathbf{J} \rangle_{\pm 1} \sim P_h(x) * P_h(-x), \quad (\text{E1})$$

where $*$ is the convolution operator. To be clear, the states $|\uparrow 0\rangle$ and $|\downarrow \pm 1\rangle$ describe the same orientation of spins in the chain, except for the two of the spins, which are flipped. Consequently, the difference on the L.H.S of this equation is equal to the subtraction $h_r - h_{r \pm 1}$, where r is the index of the particular spin considered in the chain. Finally, the PDF of the term $(h_r - h_{r \pm 1})$ is obtained from the convoluted form on the R.H.S. Note that the expectation values in the middle term correspond to the first order energy corrections, which are equal to $\langle \mathbf{J} \rangle_0 - \langle \mathbf{J} \rangle_{\pm 1} = -J$.

For the uniform distribution form of $P_h(x)$ on the interval $[-W, W]$, we have $P_h(x) * P_h(-x) = \frac{1}{2W} - \frac{|x|}{4W^2}; |x| \leq 2W$, which is shown in Figure 6(a). Therefore, the PDF for the first order energy differences $E_0^{(1)} - E_{\pm 1}^{(1)} \sim P_{E_0^{(1)} - E_{\pm 1}^{(1)}}(x)$ is obtained by shifting $P_h(x) * P_h(-x)$ by J , which is shown in Figure 6(b). Finally, the PDF of the second-order frequencies $f = \pm |E_0^{(1)} - E_{\pm 1}^{(1)}| / \hbar \sim P_F^{(2)}(f)$, is obtained by adding the value of $P_{E_0^{(1)} - E_{\pm 1}^{(1)}}(x)$ for positive energies to the reflected (about the vertical axis) values for negative energies (due to the absolute value), which is shown by a dashed blue line in Figure 6(b), followed by scaling the horizontal and vertical axes by $1/\hbar$ and \hbar respectively, which is shown in Figure 6(c).

The proof concerns a spin in the bulk of the chain. In the case of edge spins, we have $\langle \mathbf{J} \rangle_0 - \langle \mathbf{J} \rangle_{\pm 1} = -J/2$, therefore the resulting PDF, $P_F^{(2)}(f)$, must be slightly different, which can be obtained by substituting J by $\frac{J}{2}$ in the derivations and plots.

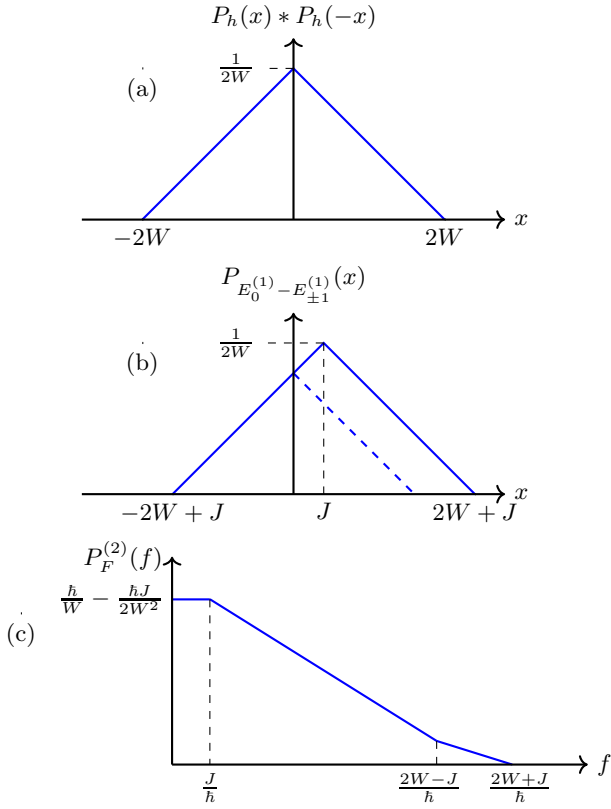


FIG. 6. Illustration of the probability density functions in E2. Each sub-figure corresponds to a step in the proof of equation 19. Sub-figure (a) shows the PDF for $E_{\uparrow 0} - E_{\downarrow \pm 1} \sim P_h(x) * P_h(-x)$. The PDF for the corrected energy difference $E_0^{(1)} - E_{\pm 1}^{(1)}$ is obtained by shifting $P_h(x) * P_h(-x)$ by J due to equation E1, which is shown in the sub-figure (b). The dashed line shows the reflected (about the vertical axis) probability densities for negative energies. Sub-figure (c) shows the PDF for the second-order frequencies in the entanglement measure $f = \pm |E_0^{(1)} - E_{\pm 1}^{(1)}|/\hbar \sim P_F^{(2)}(f)$, which is obtained by adding probability densities on the positive-energy side of the sub-figure (b), as a result of the absolute value, followed by scaling the horizontal and vertical axes by a factor of $\frac{1}{\hbar}$ and \hbar , respectively.

3. Derivation of $P_A^{(2)}(a)$

Here, we prove that equation (20) is the PDF of the amplitudes $2|c_{\pm 10}|^2 \sim P_A^{(2)}(a)$. To this end, we start by finding the Cumulative Density Function (CDF) $R_A(a) = \int_{-\infty}^a P_A^{(2)}(a') da'$:

$$\begin{aligned}
 R_A(a) &= \mathbf{P}\left\{2|c_{\pm 10}|^2 \leq a\right\} \\
 &= \mathbf{P}\left\{2\left|\frac{\langle \pm 1 | \mathbf{J} | 0 \rangle}{E_{\pm 1} - E_0}\right|^2 \leq a\right\} \\
 &= \mathbf{P}\left\{|E_{\pm 1} - E_0| \geq \frac{J}{\sqrt{2a}}\right\},
 \end{aligned} \tag{E2}$$

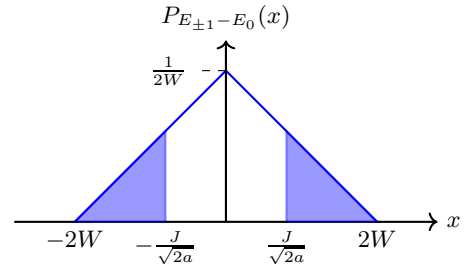


FIG. 7. Schematic illustration of the CDF (E2). This figure demonstrates the CDF $R_A(a)$, as the area below the PDF curve for the difference between the unperturbed energy levels, $P_{E_{\pm 1} - E_0}(x)$, which was previously derived in E3.

where $\mathbf{P}\{\cdot\}$ is the probability measure and we have used the fact that $|\langle \pm 1 | \mathbf{J} | 0 \rangle| = \frac{J}{2}$. This probability can be obtained from $P_{E_{\pm 1} - E_0}(x)$ calculated in the previous subsection. Figure 7 shows the area corresponding to this probability (in blue color), which is equal to:

$$R_A(a) = \left(1 - \frac{J}{2W\sqrt{2a}}\right)^2. \tag{E3}$$

Now we can obtain the PDF $P_A^{(2)}(a)$ by differentiating $R_A(a)$:

$$P_A^{(2)}(a) = \frac{d}{da} R_A(a) = \frac{W}{J} \frac{\sqrt{8a} - 1}{8\left(\frac{W}{J}a\right)^2}; \quad a \geq \frac{1}{8}\left(\frac{J}{W}\right)^2. \tag{E4}$$

Appendix F: Exponential decay of $\mathbf{P}^{(2n)}$

Here we use the Mellin transformation to show that the critical probability $\mathbf{P}^{(2n)}$ scales exponentially in the order number ($\sim (J/W)^{2n}$). To this end, according to (21) we directly obtain the PDF $\hat{P}^{(2n)}$ of the product term from the PDF of the single terms. Before proceeding to the proof, note that the dependence of terms through repeated indices manifests itself strongly in the region where it is accompanied by a decreased critical probability; Also, the critical probability is agnostic to the repeated indices in the region where the terms $|\frac{h_i - h_{i+1}}{J}|$ are small (corresponding to a large critical probability). Therefore, by neglecting the repeated indices, we obtain an upper bound on the critical probability.

In the Mellin space, the transformed PDF for the product term, $(\mathcal{M}\{\hat{P}^{(2n)}\})$ is equal to the product of the transformed PDFs of single fractions [49], which (based on the derivations in section E2) is

$$\left|\frac{h_i - h_{i+1}}{J}\right| \sim \hat{P}^{(1)}(x) = \frac{1}{W} - \frac{Jx}{2W^2}; \quad 0 \leq x \leq \frac{2W}{J}. \tag{F1}$$

Accordingly, its Mellin transformation is

$$\begin{aligned}\Phi(z) &= \mathcal{M}\{\hat{P}^{(1)}(x)\} \doteq \int_0^\infty x^{z-1} \hat{P}^{(1)}(x) dx \\ &= \frac{J}{W} \left(\frac{2W}{J}\right)^z \left(\frac{1}{z} - \frac{J/W}{z+1}\right).\end{aligned}\quad (\text{F2})$$

Based on this transformation, $\hat{P}^{(2n)}(x)$ can be obtained as follows

$$\begin{aligned}\hat{P}^{(2n)}(x) &= \mathcal{M}^{-1}\{(\Phi(z))^{2n}\} \\ &= \left(\frac{J}{W}\right)^{2n} \mathcal{M}^{-1}\left\{\left(\frac{2W}{J}\right)^{2n} z \sum_{k=0}^{2n} \binom{2n}{k} z^{k-2n} \left(\frac{-J/W}{z+1}\right)^k\right\}. \\ &= \left(\frac{J}{W}\right)^{2n} \frac{\left(\ln\left(\left(\frac{2W}{J}\right)^{2n} x^{-1}\right)\right)^{2n-1}}{\Gamma(2n)} \\ &+ \sum_{k=1}^{2n} (-1)^k \left(\frac{J}{W}\right)^{2n+k} \frac{2n}{(2n-k)!k!} \left(\frac{2W}{J}\right)^{2n} x^{-1} \frac{-1}{2} \mathbf{M}_{k-n, n-\frac{1}{2}} \left(\ln\left(\left(\frac{2W}{J}\right)^{2n} x^{-1}\right)\right) \\ &\stackrel{J \ll W}{\approx} \left(\frac{J}{W}\right)^{2n} \frac{\left(\ln\left(\left(\frac{2W}{J}\right)^{2n} x^{-1}\right)\right)^{2n-1}}{\Gamma(2n)},\end{aligned}\quad (\text{F3})$$

where $\mathbf{M}_{\nu, \mu}(\cdot)$ is the Whittaker function [52]. Therefore, we described the PDF of interest as an inverse Mellin

transformation on the R.H.S. Now, using (21), the critical probability can be obtained

$$\mathbf{P}^{(2n)} = \int_0^1 \hat{P}^{(2n)}(x) dx = \left(\frac{J}{W}\right)^{2n} \frac{1}{\Gamma(2n)} \left[x \sum_{l=0}^{2n-1} \frac{(2n-1)!}{l!} \left(\ln\left(\left(\frac{2W}{J}\right)^{2n} x^{-1}\right)\right)^l \right]_0^1 \approx \left(\frac{J}{W}\right)^{2n} \frac{(2n \ln\left(\frac{2W}{J}\right))^{2n-1}}{(2n-1)!}. \quad (\text{F4})$$

Thus, using the Stirling's approximation, $\ln((2n-1)!) \approx$

$(2n-1)(\ln(2n-1) - 1)$, we have

$$\ln(\mathbf{P}^{(2n)}) \approx 2n \ln\left(\frac{J}{W}\right) + (2n-1) \left(\ln\left(\frac{2n \ln\left(\frac{2W}{J}\right)}{2n-1}\right) + 1\right). \quad (\text{F5})$$

-
- [1] A. M. Kaufman, M. E. Tai, A. Lukin, M. Rispoli, R. Schittko, P. M. Preiss, and M. Greiner, Quantum thermalization through entanglement in an isolated many-body system, *Science* **353**, 794 (2016).
 [2] S. Trotzky, Y.-A. Chen, A. Flesch, I. P. McCulloch, U. Schollwöck, J. Eisert, and I. Bloch, Probing the relaxation towards equilibrium in an isolated strongly correlated one-dimensional bose gas, *Nature physics* **8**, 325 (2012).
 [3] T. Langen, R. Geiger, M. Kuhnert, B. Rauer, and

- J. Schmiedmayer, Local emergence of thermal correlations in an isolated quantum many-body system, *Nature Physics* **9**, 640 (2013).
 [4] H. Li and F. D. M. Haldane, Entanglement spectrum as a generalization of entanglement entropy: Identification of topological order in non-abelian fractional quantum hall effect states, *Phys. Rev. Lett.* **101**, 010504 (2008).
 [5] S. Popescu, A. J. Short, and A. Winter, Entanglement and the foundations of statistical mechanics, *Nature Physics* **2**, 754 (2006).

- [6] M. Srednicki, Chaos and quantum thermalization, *Physical Review E* **50**, 888 (1994).
- [7] J. M. Deutsch, Quantum statistical mechanics in a closed system, *Physical Review A* **43**, 2046 (1991).
- [8] M. Rigol, V. Dunjko, and M. Olshanii, Thermalization and its mechanism for generic isolated quantum systems, *Nature* **452**, 854 (2008).
- [9] J. Eisert, M. Friesdorf, and C. Gogolin, Quantum many-body systems out of equilibrium, *Nature Physics* **11**, 124 (2015).
- [10] L. D'Alessio, Y. Kafri, A. Polkovnikov, and M. Rigol, From quantum chaos and eigenstate thermalization to statistical mechanics and thermodynamics, *Advances in Physics* **65**, 239 (2016), <https://doi.org/10.1080/00018732.2016.1198134>.
- [11] H. Bernien, S. Schwartz, A. Keesling, H. Levine, A. Omran, H. Pichler, S. Choi, A. S. Zibrov, M. Endres, M. Greiner, *et al.*, Probing many-body dynamics on a 51-atom quantum simulator, *Nature* **551**, 579 (2017).
- [12] A. Pal and D. A. Huse, Many-body localization phase transition, *Physical review b* **82**, 174411 (2010).
- [13] D. M. Basko, I. L. Aleiner, and B. L. Altshuler, Metal-insulator transition in a weakly interacting many-electron system with localized single-particle states, *Annals of physics* **321**, 1126 (2006).
- [14] C. Holzhey, F. Larsen, and F. Wilczek, Geometric and renormalized entropy in conformal field theory, *Nuclear Physics B* **424**, 443 (1994).
- [15] P. Calabrese and J. Cardy, Entanglement entropy and quantum field theory, *Journal of Statistical Mechanics: Theory and Experiment* **2004**, P06002 (2004).
- [16] P. Calabrese and J. Cardy, Evolution of entanglement entropy in one-dimensional systems, *Journal of Statistical Mechanics: Theory and Experiment* **2005**, P04010 (2005).
- [17] P. Calabrese and J. Cardy, Entanglement entropy and conformal field theory, *Journal of Physics A: Mathematical and Theoretical* **42**, 504005 (2009).
- [18] N. Lashkari, A. Dymarsky, and H. Liu, Eigenstate thermalization hypothesis in conformal field theory, *Journal of Statistical Mechanics: Theory and Experiment* **2018**, 033105 (2018).
- [19] A. Dymarsky and K. Pavlenko, Generalized eigenstate thermalization hypothesis in 2d conformal field theories, *Phys. Rev. Lett.* **123**, 111602 (2019).
- [20] D. Pekker, G. Refael, E. Altman, E. Demler, and V. Oganesyan, Hilbert-glass transition: New universality of temperature-tuned many-body dynamical quantum criticality, *Phys. Rev. X* **4**, 011052 (2014).
- [21] R. Vosk and E. Altman, Dynamical quantum phase transitions in random spin chains, *Phys. Rev. Lett.* **112**, 217204 (2014).
- [22] M. Rispoli, A. Lukin, R. Schittko, S. Kim, M. E. Tai, J. Léonard, and M. Greiner, Quantum critical behaviour at the many-body localization transition, *Nature* **573**, 385 (2019).
- [23] E. Fradkin, *Field theories of condensed matter physics* (Cambridge University Press, 2013).
- [24] P. W. Anderson, Absence of diffusion in certain random lattices, *Physical review* **109**, 1492 (1958).
- [25] L. Fleishman and P. Anderson, Interactions and the anderson transition, *Physical Review B* **21**, 2366 (1980).
- [26] V. Oganesyan and D. A. Huse, Localization of interacting fermions at high temperature, *Phys. Rev. B* **75**, 155111 (2007).
- [27] M. Serbyn, Z. Papić, and D. A. Abanin, Criterion for many-body localization-delocalization phase transition, *Phys. Rev. X* **5**, 041047 (2015).
- [28] V. Khemani, S. P. Lim, D. N. Sheng, and D. A. Huse, Critical properties of the many-body localization transition, *Phys. Rev. X* **7**, 021013 (2017).
- [29] R. Vosk, D. A. Huse, and E. Altman, Theory of the many-body localization transition in one-dimensional systems, *Phys. Rev. X* **5**, 031032 (2015).
- [30] A. C. Potter, R. Vasseur, and S. A. Parameswaran, Universal properties of many-body delocalization transitions, *Phys. Rev. X* **5**, 031033 (2015).
- [31] A. Goremykina, R. Vasseur, and M. Serbyn, Analytically solvable renormalization group for the many-body localization transition, *Phys. Rev. Lett.* **122**, 040601 (2019).
- [32] A. Morningstar, D. A. Huse, and J. Z. Imbrie, Many-body localization near the critical point, *Phys. Rev. B* **102**, 125134 (2020).
- [33] A. Kshetrimayum, M. Goihl, and J. Eisert, Time evolution of many-body localized systems in two spatial dimensions, *Physical Review B* **102**, 235132 (2020).
- [34] E. Chertkov, B. Villalonga, and B. K. Clark, Numerical evidence for many-body localization in two and three dimensions, *Physical Review Letters* **126**, 180602 (2021).
- [35] E. V. H. Doggen, I. V. Gornyi, A. D. Mirlin, and D. G. Polyakov, Slow many-body delocalization beyond one dimension, *Phys. Rev. Lett.* **125**, 155701 (2020).
- [36] V. Khemani, S.-P. Lim, D. Sheng, and D. A. Huse, Critical properties of the many-body localization transition, *Physical Review X* **7**, 021013 (2017).
- [37] R. Nandkishore and D. A. Huse, Many-body localization and thermalization in quantum statistical mechanics, *Annu. Rev. Condens. Matter Phys.* **6**, 15 (2015).
- [38] V. Oganesyan and D. A. Huse, Localization of interacting fermions at high temperature, *Physical review b* **75**, 155111 (2007).
- [39] S. Garratt and J. Chalker, Many-body delocalization as entanglement breaking, *Physical Review Letters* **127**, 026802 (2021).
- [40] A. Lukin, M. Rispoli, R. Schittko, M. E. Tai, A. M. Kaufman, V. Khemani, J. Léonard, and M. Greiner, Probing entanglement in a many-body-localized system, *Science* **364**, 256 (2019).
- [41] M. Serbyn, Z. Papić, and D. A. Abanin, Local conservation laws and the structure of the many-body localized states, *Physical review letters* **111**, 127201 (2013).
- [42] M. Serbyn, Z. Papić, and D. A. Abanin, Universal slow growth of entanglement in interacting strongly disordered systems, *Physical review letters* **110**, 260601 (2013).
- [43] D. A. Huse, R. Nandkishore, and V. Oganesyan, Phenomenology of fully many-body-localized systems, *Physical Review B* **90**, 174202 (2014).
- [44] E. J. Heller, Bound-state eigenfunctions of classically chaotic hamiltonian systems: Scars of periodic orbits, *Phys. Rev. Lett.* **53**, 1515 (1984).
- [45] M. V. Berry, Regular and irregular semiclassical wavefunctions, *Journal of Physics A: Mathematical and General* **10**, 2083 (1977).
- [46] A. Pal and D. A. Huse, Many-body localization phase transition, *Phys. Rev. B* **82**, 174411 (2010).
- [47] D. J. Luitz, N. Laflorencie, and F. Alet, Many-body localization edge in the random-field heisenberg chain, *Phys. Rev. B* **91**, 081103 (2015).
- [48] T. Devakul and R. R. P. Singh, Early breakdown of area-

- law entanglement at the many-body delocalization transition, *Phys. Rev. Lett.* **115**, 187201 (2015).
- [49] J. Galambos and I. Simonelli, *Products of random variables: applications to problems of physics and to arithmetical functions* (CRC press, 2004).
- [50] D. Basko, I. Aleiner, and B. Altshuler, Metal–insulator transition in a weakly interacting many-electron system with localized single-particle states, *Annals of Physics* **321**, 1126 (2006).
- [51] S. Nezami and M. Walter, Multipartite entanglement in stabilizer tensor networks, *Physical Review Letters* **125**, 241602 (2020).
- [52] F. Oberhettinger, *Tables of Mellin transforms* (Springer Science & Business Media, 2012).